


Predicting functional effect of missense variants using graph attention neural networks

Received: 9 July 2021

Accepted: 7 October 2022

Published online: 15 November 2022

 Check for updates

Haicang Zhang¹, Michelle S. Xu², Xiao Fan^{1,3}, Wendy K. Chung^{3,4} & Yufeng Shen^{1,5,6}  

Accurate prediction of damaging missense variants is critically important for interpreting a genome sequence. Although many methods have been developed, their performance has been limited. Recent advances in machine learning and the availability of large-scale population genomic sequencing data provide new opportunities to considerably improve computational predictions. Here we describe the graphical missense variant pathogenicity predictor (gMVP), a new method based on graph attention neural networks. Its main component is a graph with nodes that capture predictive features of amino acids and edges weighted by co-evolution strength, enabling effective pooling of information from the local protein context and functionally correlated distal positions. Evaluation of deep mutational scan data shows that gMVP outperforms other published methods in identifying damaging variants in *TP53*, *PTEN*, *BRCA1* and *MSH2*. Furthermore, it achieves the best separation of de novo missense variants in neurodevelopmental disorder cases from those in controls. Finally, the model supports transfer learning to optimize gain- and loss-of-function predictions in sodium and calcium channels. In summary, we demonstrate that gMVP can improve interpretation of missense variants in clinical testing and genetic studies.


Missense variants are major contributors to genetic risk of cancers^{1,2} and developmental disorders^{3–5}. Missense variants have been used, along with protein-truncating variants, to implicate new risk genes and are responsible for many clinical genetic diagnoses; however, the majority of rare missense variants are probably benign or only have minimal functional impact. As a result of the uncertainty of the functional impact, most rare missense variants reported in clinical genetic testing are classified as variants of uncertain significance⁶, leading to ambiguity, confusion, overtreatment and missed opportunities for clinical intervention. In human genetic studies to identify new risk genes by rare variants, pre-selecting damaging missense variants on

the basis of computational prediction is a necessary step to improve statistical power^{4,5,7,8}. Computational methods are therefore critically important to interpret missense variants in clinical genetics and disease gene discovery studies.

Numerous methods such as Polyphen⁹, SIFT¹⁰, CADD¹¹, REVEL¹², MetaSVM¹³, M-CAP¹⁴, Eigen¹⁵, MVP¹⁶, PrimateAI¹⁷, model predictive control (MPC)¹⁸ and correct classification rates (CCR)¹⁹ have been developed to address the problem. These methods differ in several aspects such as the prediction features, how the features are represented in the model, the training datasets and how the model is trained. Sequence conservation or local protein structural properties are the

¹Department of Systems Biology, Columbia University, New York, NY, USA. ²Columbia College, Columbia University, New York, USA.

³Department of Pediatrics, Columbia University, New York, NY, USA. ⁴Department of Medicine, Columbia University, New York, NY, USA.

⁵Department of Biomedical Informatics, Columbia University, New York, NY, USA. ⁶JP Sulzberger Columbia Genome Center, Columbia University, New York, NY, USA.  e-mail: ys2411@cumc.columbia.edu

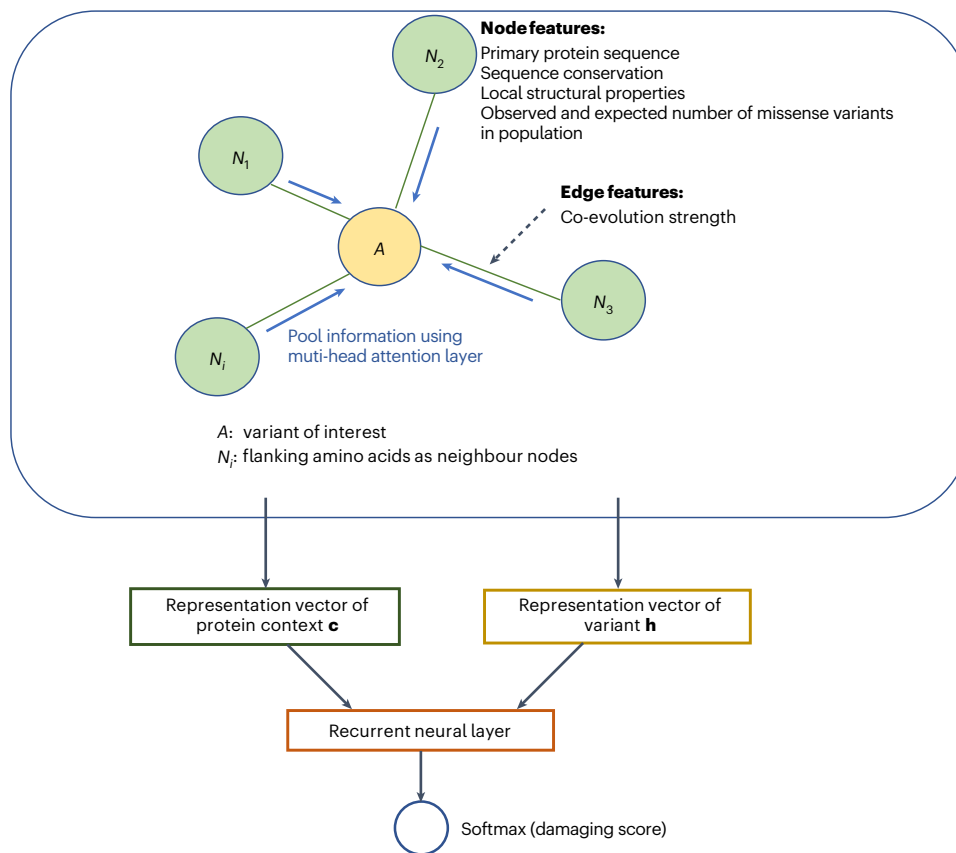


Fig. 1 | An overview of gMVP model. gMVP uses a graph to represent a variant and its protein context defined as 128 amino acids flanking the reference amino acid. The amino acid of interest is the centre node (coloured orange) and the flanking amino acids are the context nodes (coloured light green). All context nodes are connected with the centre node but not each other. The edge feature is co-evolution strength. The node features include conservation and predicted structural properties. Centre node features also include the amino

acid substitution; context node features include the primary sequence and the expected and observed number of rare missense variants in human population. We use three one-depth dense layers to encode the input features to latent representation vectors and used a multi-head attention layer to learn context vector **c**. We then use a recurrent neural layer connected with softmax layer to generate prediction score from **c** and the representation vector **h** of variant.

main prediction features for early computational methods such as GERP²⁰ and PolyPhen. The MPC and CCR methods estimate sub-genic coding constraints from large human population sequencing data, providing additional information not captured by past methods. PrimateAI learns the protein context from sequences and local structural properties using deep representation learning. A number of studies have reported evidence that functionally damaging missense variants are clustered in three-dimensional protein structures^{21–23}. Co-evolution captures the functional correlation between positions. Recent studies^{24,25} have shown that co-evolution helps to improve the prediction accuracy.

Here we present the graphical missense variant pathogenicity predictor (gMVP), a graph attention neural network model designed to effectively represent or learn the representation of all of the information sources to improve prediction of the functional impact of missense variants. gMVP uses a graph to represent a variant and its protein context, with node features describing sequence conservation and local structural properties; it also uses a graph attention neural network to learn the representation of a large protein context and uses the co-evolution strength as edge features that can potentially pool information about conservation and coding constraints of distant but functionally correlated positions. We trained gMVP using curated pathogenic variants and random rare missense variants in the human population. We then benchmarked the performance using datasets that have been curated or collected by entirely different approaches,

for example: cancer somatic mutation hotspots²⁶; functional read-out datasets from deep mutational scan studies of well-known risk genes^{27–30}; and de novo missense variants (DNMs) from studies of autism spectrum disorder (ASD)⁴ and neurodevelopmental disorder (NDD)⁵. Finally, we investigated the potential utility of transfer learning for classifying gain-of-function (GOF) and loss-of-function (LOF) variants in specific gene families based on the generic model trained across all genes.

Results

Model architecture and prediction features

gMVP is a supervised machine learning method for predicting functionally damaging missense variants. The functional consequence of missense variants depends on both the type of amino acid substitution and its protein context. gMVP uses a graph attention neural network to learn representation of protein sequence and structure context and context-dependent impact of amino acid substitutions on protein function.

The main component of gMVP is a graph that represents a variant and its protein context (Fig. 1 and Supplementary Fig. 1). Given a variant, we define the 128 amino acids flanking the reference amino acid as protein context. We note that the average length of a protein domain annotated in the UniProt database is about 110 amino acids (Supplementary Fig. 8). We build a star-like graph with the reference amino acid as the centre node and the flanking amino acids as context nodes

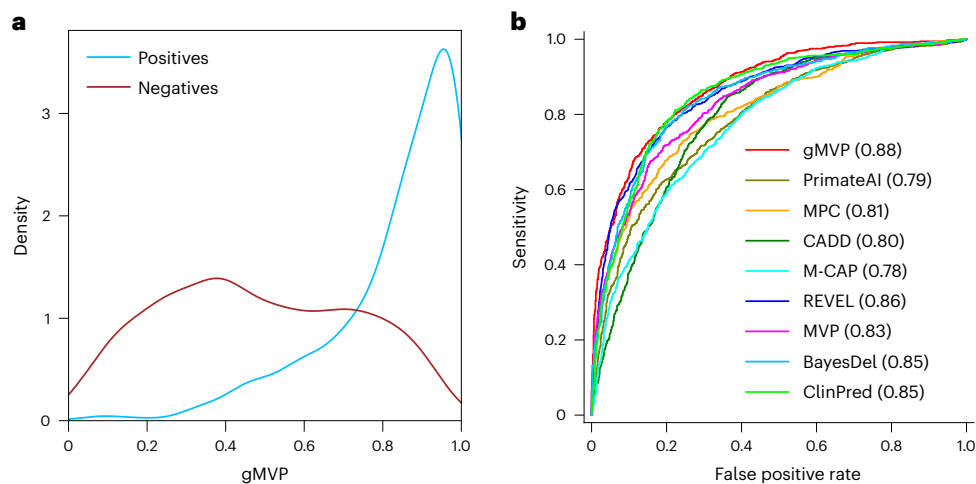


Fig. 2 | Evaluating gMVP and published methods using cancer somatic mutation hotspots and random variants in population. a, The gMVP score distributions for variants in cancer hotspots (labelled positives) and random missense variants in population (labelled negatives). **b**, Comparisons between

the ROC curves of gMVP and other published methods. The ROC curves are evaluated on 878 cancer mutations located in hotspots from 209 genes and 1,756 (that is, a twofold greater number of positives) randomly selected rare variants from the DiscovEHR data.

and connect the centre node and every context node with edges. We use co-evolution strength between the centre node of the variant and the context node as edge features. The co-evolution strength is highly correlated with functional interactions and protein residue–residue contact that captures the potential three-dimensional neighbours in folded proteins^{24,25,31,32}. This architecture therefore allows the model to directly represent interactions between the position of interest and each flanking position in a wide context window. For the centre node, we include the amino acid substitution, evolutionary sequence conservation, and predicted local structural properties, such as secondary structures, as features (Methods). For context nodes, in addition to primary sequence, sequence conservation and local structure features, we also include the expected and observed number of rare missense variants in the human population to capture the selection effect of damaging variants in humans^{18,19}. Let \mathbf{x} , $\{\mathbf{n}_i\}$ and $\{\mathbf{f}_i\}$ denote input feature vectors for the centre node, neighbour nodes and edges, respectively. We first use three one-depth dense layers to encode \mathbf{x} , $\{\mathbf{n}_i\}$ and $\{\mathbf{f}_i\}$ to latent representation vectors \mathbf{h} , $\{\mathbf{t}_i\}$ and $\{\mathbf{e}_i\}$, respectively. We then use a multi-head attention layer to learn the attention weight w_i for each neighbour and to learn a context vector \mathbf{c} by weighting the neighbours. Attention scores play a key part in attention-based neural networks^{33,34}. Our attention scores account for both the node features and the edge features. Specifically, we use $\tanh(\mathbf{W}[\mathbf{h}, \mathbf{t}_i, \mathbf{e}_i])$ as attention scores, where \tanh denotes a hyperbolic tangent activation function, and \mathbf{W} is the weight matrix to be trained. We next used a gated recurrent layer³⁵—which is widely used to leverage sequence context in natural language modelling—to integrate vectors \mathbf{c} and \mathbf{h} of the variant. Finally, we use a linear layer and a sigmoid layer to perform classification and output the damaging scores.

Model training and testing

We collected likely pathogenic and benign missense variants from curated databases (HGMD³⁶, ClinVar³⁷ and UniProt³⁸) as training positives and negatives, respectively, and excluded the variants with conflicting evidence in the databases (Methods). To balance the positive and negative sets, we randomly selected rare missense variants observed in human population sequencing data DiscovEHR as additional negatives for training. In total there are 59,701 positives and 59,701 negatives, which cover 3,463 and 14,222 genes, respectively. We used a stochastic gradient descent algorithm³⁹ to update the model's parameters at an initial learning rate of 1×10^{-3} and applied

early stopping with validation loss as a metric to avoid overfitting. We implemented the model and training algorithms using TensorFlow⁴⁰. The whole training process took ~4 h on a Linux workstation with one NVIDIA Titan RTX GPU. When benchmarking the performance using a range of datasets, we compared gMVP with other widely used methods in genetic studies such as PrimateAI¹⁷, M-CAP¹⁴, CADD¹¹, MPC¹⁸, REVEL¹², MVP¹⁶, ClinPred⁴¹ and BayesDel⁴².

Human-curated pathogenic variants have hidden false positives that are probably caused by systematic biases and errors, which can be picked up by deep neural networks; therefore, conventional approaches for performance evaluation, using testing data randomly partitioned from the same source as the training data, usually lead to an inflated performance measure. To objectively evaluate the performance of the model, we compiled cancer somatic mutations that are unlikely to share the same systematic errors as the training datasets. We included missense mutations located in inferred hotspots on the basis of statistical evidence from a recent study²⁶ as positives and randomly selected rare variants from the DiscovEHR database⁴³ as negatives. The gMVP score distributions of cancer hotspot mutations and random variants have distinct modes (Fig. 2a). We selected a threshold of 0.75 to indicate a binary prediction for other downstream analyses that can best separate the score distributions of the positives and negatives. When compared with other published methods, gMVP achieved the best performance with an area under the receiver operating characteristic curve (AUROC) of 0.88 (Fig. 2b and Supplementary Table 2). REVEL is close with an AUROC of 0.86.

gMVP can identify damaging variants in known disease genes

Missense variants that occur in different protein contexts—even in the same gene—can have different impacts. This is the core problem in interpreting variants from known risk genes in clinical genetic testing and the discovery of new disease genes. As performance evaluation using variants across genes is confounded by gene-level properties, here we aim to evaluate the ability of gMVP and other methods to distinguish damaging variants from neutral variants in the same genes. To this end, we obtained functional readout data from deep mutational scan assays of four well-known disease risk genes, *TP53*³⁰, *PTEN*²⁹, *BRCA1*²⁸ and *MSH2*²⁷, as benchmark data. The data include 432 damaging (positives) and 1,476 neutral (negatives) variants for *BRCA1*; 262 positives and 1,632 negatives for *PTEN*; 540 positives and 1,108 negatives for *TP53*; and 414 positives and 5,439 negatives for *MSH2*, respectively.

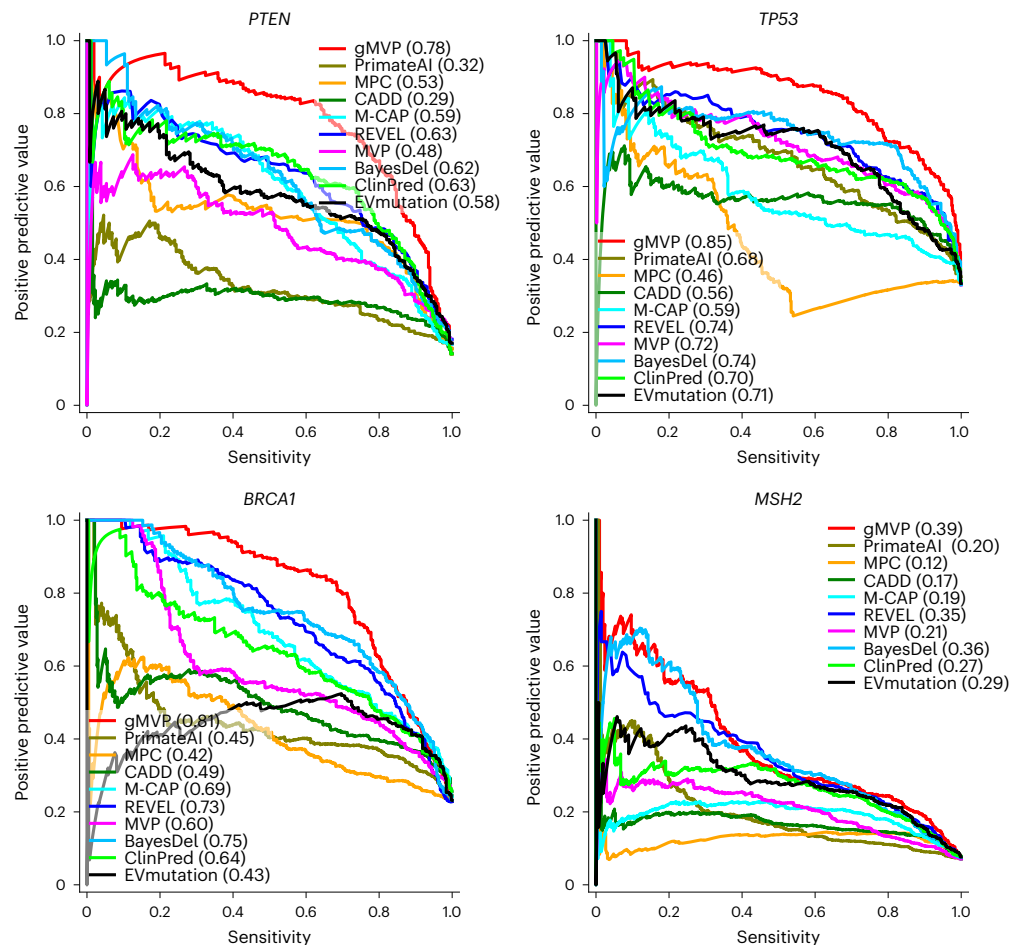


Fig. 3 | Evaluating gMVP and published methods in identifying damaging variants in known disease genes such as *TP53*, *PTEN*, *BRCA1* and *MSH2*. The precision–recall curves of gMVP and published methods are shown for each gene using functional readout data—labelled on the basis of the recommended threshold—as the ground truth.

We note that all variants in these four genes were excluded during gMVP training to avoid inflation in performance evaluation.

We first investigated the gMVP score distributions of damaging and neutral variants. Damaging variants clearly have different score distribution compared with the neutral variants in each gene (Supplementary Fig. 2). gMVP scores are also highly correlated with functional scores from the deep mutational scan assays, with a Spearman correlation coefficient of 0.67 ($P = 1 \times 10^{-246}$), -0.48 ($P = 8 \times 10^{-122}$), -0.53 ($P = 7 \times 10^{-51}$) and 0.29 ($P = 7 \times 10^{-117}$) in *TP53*, *PTEN*, *BRCA1* and *MSH2*, respectively (Supplementary Fig. 3 and Supplementary Table 3–6).

We then used functional readout data as the ground truth to estimate precision–recall and compared gMVP with other methods. The areas under the precision–recall curves (AUPRCs) of gMVP are 0.78, 0.85, 0.81 and 0.39 for *PTEN*, *TP53*, *BRCA1* and *MSH2*, respectively (Fig. 3), whereas the AUPRCs of the second-best method (REVEL) are 0.63, 0.74, 0.73 and 0.35, respectively. PrimateAI, a recent deep representation learning-based method, has AUPRCs of 0.32, 0.68, 0.45 and 0.20, respectively. A comparison using receiver operating characteristic (ROC) curves shows similar patterns (Supplementary Fig. 4).

Prioritizing rare DNMs using gMVP

To further evaluate the utility of gMVP in new risk gene discovery, we compared the gMVP scores of DNMs from cases with developmental disorders with those from controls. We obtained published DNMs from 5,924 cases in an ASD study⁴, from 31,058 cases in an NDD study⁵ and from 2,007 controls (unaffected siblings from the ASD study)⁴.

Although there is no ground truth because most of these DNMs were not previously implicated with diseases, there is a substantial excess of such variants in cases compared with the controls^{3,44,45}, suggesting that a substantial fraction of variants in cases are pathogenic. We therefore tested whether the predicted scores of variants in cases and controls are significantly different and used significance as a proxy of performance (Fig. 4a). gMVP achieves a P -value of 38×10^{-9} and 28×10^{-40} for ASD or NDD versus controls, respectively, whereas the second-best method PrimateAI achieves a P -value of 38×10^{-6} and 28×10^{-38} , respectively (Supplementary Fig. 5).

We then calculated the enrichment rate of predicted damaging DNMs of a method with a certain threshold in cases compared with the controls, and then estimated the precision and the number of true risk variants (Methods), which is a proxy of recall because the total number of true positives in all cases is a (unknown) constant that is independent of the methods. The estimated precision and recall values are directly related to the power of detecting new risk genes^{5,46}. We also calculated the estimated precision and number of true risk variants on all missense variants (denoted as All Mis) in the dataset, without using any predictor. We compared the performance of gMVP with other methods by the estimated precision and recall–proxy curves (Fig. 4b,c). The optimal threshold of the gMVP rank score in cancer hotspots is 0.75; with this, we observed an enrichment rate of 2.7 and 1.5 in NDD and ASD, respectively (Supplementary Tables 7 and 8), which corresponds to an estimated precision–recall of (0.62, 4,818) and (0.35, 328), respectively. Furthermore, when using a lower threshold of 0.7,

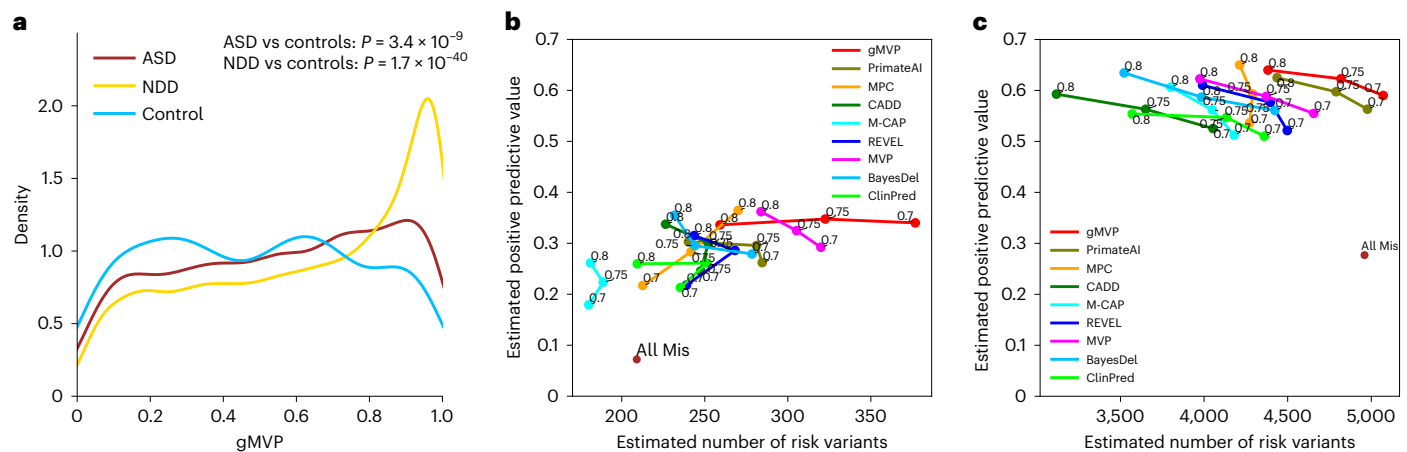


Fig. 4 | Evaluating gMVP and published methods in distinguishing rare DNMs in cases with neurodevelopmental disorders from those in controls. **a**, Distributions of gMVP-predicted scores for rare DNMs from ASD and NDD cases, as well as controls. We used a two-sided Mann–Whitney *U* test to assess the statistical significance of the difference between the cases and controls. Controls are unaffected siblings from the ASD study. **b**, Comparisons between gMVP and

other published methods using DNMs from ASD cases and controls by precision–recall–proxy curves. Numbers on each point indicate rank percentile thresholds. The positions of the All Mis points are estimated from all missense variants without using any prediction method. **c**, The same comparison using data from NDD cases and controls.

gMVP can still keep the precision as high as 0.34, and achieved a recall of 377 in ASD. PrimateAI achieves overall second-best estimated precision and recall under different thresholds in both ASD and NDD. MPC, with a threshold of 0.8, can reach a high precision at 0.65 and 0.36 in NDD and ASD, respectively, but overall it has substantially lower recall than gMVP and PrimateAI.

Classifying mode of action of variants via transfer learning

In many genes, the functional impact of missense variants is complex and cannot be simply captured by a binary prediction. Heyne et al.⁴⁷ recently investigated the pathogenetic variants that alter the channel activity of voltage-gated sodium and calcium channels and inferred LOF and GOF variants on the basis of clinical phenotypes of variant carriers and electrophysiology data. The study also described a computational model (funNCion) to predict LOF and GOF variants using a large number of human-curated features on electrophysiological properties. Here we sought to classify LOF and GOF variants using the gMVP model through transfer learning without additional curated prediction features. Transfer learning allows us to further train a model for a specific purpose using a limited number of training points by only exploring a reasonable subspace of the whole parameter spaces guided by previously trained models.

We obtained 1,517 pathogenetic and 2,328 neutral variants in ten voltage-gated sodium and ten calcium channel genes, in which 518 and 309 variants were inferred as LOF and GOF variants, respectively, from the work by Heyne and colleagues⁴⁷. To benchmark the performance, we used the same training and testing sets (90/10% breakdown) as funNCion.

We first evaluated the performance of gMVP and previous methods in distinguishing LOF or GOF from neutral variants. gMVP and REVEL both achieved the best AUROC of 0.94 (Fig. 5a and Supplementary Table 9). FunNCion⁴⁷, which was trained specifically on the variants of the ion-channel genes, achieved a nearly identical AUROC of 0.93. We next sought to improve the performance using transfer learning. Starting with the weights from the original gMVP model, we trained a new model, gMVP-TL1, with both LOF and GOF variants in these genes as positives, and neutral variants as negatives (Methods). gMVP-TL1 achieved an AUROC of 0.96, outperforming the original gMVP and published methods. Furthermore, to distinguish LOF and GOF variants, we trained another model, gMVP-TL2, also starting with the weights of

the original gMVP model, but with different output labels for training (LOF versus GOF; Methods). The training set includes 465 LOF and 279 GOF variants, whereas the testing set comprises 51 LOF and 30 GOF variants. gMVP-TL2 achieved an AUROC of 0.95, substantially better than funNCion (AUROC, 0.84), which trained on the same variants set with manually curated prediction features (Fig. 5b and Supplementary Table 10). This demonstrates that the gMVP model aided by transfer learning technique can accurately predict GOF and LOF variants in channel genes with a very limited training dataset.

gMVP captures conservation, structure and selection in humans

We calculated the correlation between predicted scores of gMVP and other methods on DNMs from ASD and NDD cases and controls (Fig. 6a). gMVP has the highest correlation with REVEL (Spearman $\rho = 0.78$), followed by a few other widely used methods such as BayesDel, MPC, CADD and PrimateAI ($\rho > 0.6$).

We then performed principal component analysis (PCA) on the DNMs from cases and controls to investigate the contributing factors that separate the variants (Fig. 6b and Supplementary Fig. 6). The input of the PCA is a score matrix in which rows represent variants and columns represent predicted scores by gMVP and other methods. We included two additional columns with gene-level gnomAD constraint metrics o/e-LoF and o/e-Mis (observed number over expected number for LOF and missense)⁴⁸ to represent selection effect in humans. The first component (PC1) captures the majority of the variance of the data and best separates the DNMs in cases and the ones in controls. All methods have large loadings on PC1 (Fig. 6b). The second component (PC2) is largely driven by the gene-level gnomAD constraint metrics (Fig. 6b). The joint distribution of PC1/2 scores of DNMs from controls has a single mode at the centre. The joint distributions of scores of DNMs from cases have two modes (Fig. 6b and Supplementary Fig. 6b) that represent mixtures of likely pathogenic variants and random DNMs. Notably, gnomAD metrics have near orthogonal loadings on PC1/2 with GERP, which is purely based on cross-species conservation, suggesting that selection effect in humans provides complementary information to evolutionary conservation about genetic effect of missense variants. All methods (PolyPhen, eigen, CADD, VEST and REVEL) that do not use human or primate population genome data have loadings close to GERP on PC1/2. MPC and M-CAP, which use sub-genic or gene-level mutation

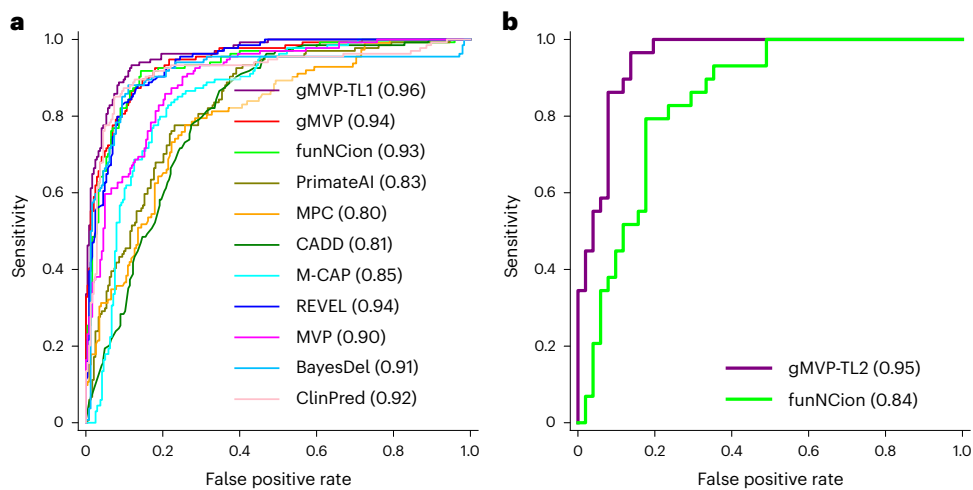


Fig. 5 | Evaluating gMVP and other published methods in classifying pathogenic and neutral variants, and in predicting GOF and LOF variants in ion-channel genes. a, Comparison of ROC curves in classifying pathogenic variants and neutral variants. gMVP-TL1 denotes the model further trained on

the pathogenic and neutral variants in *SCN4A* genes starting from the weights of the original gMVP model. **b,** Comparison of ROC curves in classifying GOF and LOF variants. gMVP-TL2 denotes the model further trained on GOF and LOF variants starting from the weights of the original gMVP model.

intolerance metrics similar to gnomAD metrics, have the closest loadings as gnomAD metrics on PC1/2. gMVP and PrimateAI have similar loadings that are in the middle of GERP and gnomAD metrics.

We inspected the *BRCT2* domain of *BRCA1* to show how the gMVP model captures context-dependent functional impact. We observed that most damaging variants predicted by gMVP (>0.75) are located in the core region of *BRCT2* domain (Fig. 6c). Furthermore, gMVP scores are highly correlated with evolutionary conservation (Fig. 6d and Supplementary Fig. 7a; $\rho = 0.57$). Variants in the β -sheets are much more damaging than the ones in α -helix regions, and the ones in α -helix regions are more damaging than the ones in coil regions (Fig. 6d and Supplementary Fig. 7b), consistent with past discoveries^{21,49,50}. Finally, amino acids mutated to proline (P) in helix regions are predicted to be highly damaging, even in positions not well conserved (Fig. 6d). This is consistent with the fact that proline rarely occurs in the middle of an α -helix⁵¹.

Discussion

We developed gMVP—a new method based on graph attention neural networks—to predict functionally damaging missense variants. gMVP uses attention neural networks to learn representations of protein sequence and structure context through supervised learning trained with large number of curated pathogenic variants. The graph structure allows co-evolution-guided pooling of predictive information of distal amino acid positions that are functionally correlated or potentially close in three-dimensional space. We demonstrated the utility of the gMVP in clinical genetic testing and new risk gene discovery studies. Specifically, we showed that gMVP achieves better accuracy in identification of damaging variants in known risk genes based on functional readout data from deep mutational scan studies. Furthermore, gMVP achieved better performance in prioritizing DNMs in cases with autism or NDD, suggesting that it can be used to pre-select damaging variants or weight variants to improve statistical power of new risk gene discovery. Finally, we showed that with transfer learning technique, gMVP model can accurately classify GOF and LOF variants in ion channels even with a limited training set without additional prediction features.

gMVP learns a representation of protein context from training data, whereas previous ensemble methods such as REVEL, M-CAP, MetaSVM and CADD used scores from other predictors or other human-engineered features as inputs. With recent progress of machine learning in protein structure prediction^{52–55}, neural network

representations could capture latent structure beyond common linear representations of understanding of the biophysical and biochemical properties. We showed that representation learning allows gMVP to capture the context-dependent impact of amino acid substitutions on protein function. PrimateAI is a recently published method that also uses deep representation learning. gMVP achieved better performance than PrimateAI in identification of damaging variants in known disease risk genes in comparisons that use functional readout data as well as in prioritizing rare DNMs from ASD and NDD studies. Although both models used evolutionary conservation and protein structural properties as features, the two methods have entirely different model architecture and training data. gMVP uses a graph attention neural network to pool information from both distal and local positions with co-evolution strength, whereas PrimateAI uses a convolutional neural network to extract local patterns from a protein context. For training data, gMVP used expert-curated variants and random variants in population as training positives and negatives, respectively. By contrast, PrimateAI used common variants in primates as negatives and unobserved variants in the population as positives. Based on functional readout data of the four well-known risk genes, only 15–25% of random variants have discernible impact on protein function. The positives used in PrimateAI training may therefore contain a large fraction of false positives. PrimateAI's training strategy does have advantages. It avoids human interpretation bias and errors in curated databases of pathogenic variants, the positives used in gMVP training. It also can cover almost all human protein-coding genes, whereas curated databases such as ClinVar only cover hundreds of genes. Additionally, common variants in primates are probably all true negatives, whereas random observed rare variants in human population could have a non-negligible fraction of damaging variants. Making a new model that can use all of these datasets in training could further improve the prediction performance.

Several past studies have shown that the functional impact of missense variants is correlated among three-dimensional neighbours^{21,22,56}. Pooling information from three-dimensional neighbours could therefore improve predictions of functional impact. However, directly considering three-dimensional distances is limited by the fact that most human proteins have no solved tertiary structures with considerable coverage. gMVP addresses this issue by taking a large segment of the protein context that include both local and distant positions that are potential neighbours in folded proteins, and then

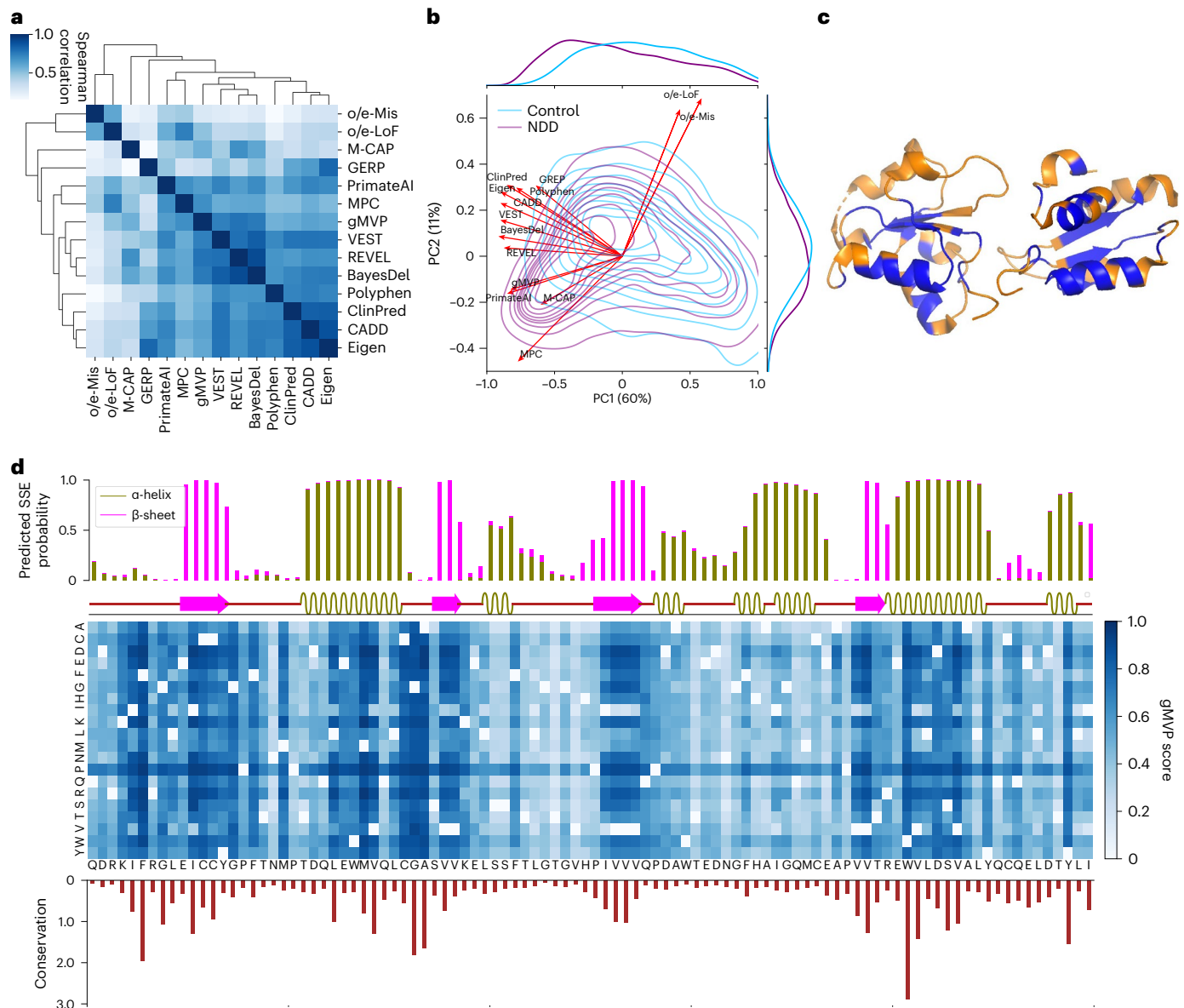


Fig. 6 | Interpreting gMVP predictions with conservation, protein structure and genetic coding constraints.

a, Spearman correlation between gMVP and other published methods, calculated by scores of the DNMs in ASD, NDD and controls. **b**, PCA on DNMs from ASD and NDD cases and controls. Red arrows show the loadings of gMVP and published methods on the first two components; the density contour shows the distribution of PC1/2 scores of the variants in NDD and controls. The density curves along the axes show the distribution of PC1 or PC2 scores of the cases and controls. **c**, The protein tertiary structure of BRTC2 domain of BRCA1. We coloured a residue blue if at least one missense on

this position is predicted to be damaging (gMVP > 0.75) and orange otherwise. **d**, gMVP scores of all possible missense variants on the BRTC2 domain of BRCA1. The top bar plot shows the predicted probabilities of the protein secondary structures, whereas the bar below shows the real protein secondary structures calculated by DSSP. The middle heatmap shows gMVP scores for all possible missense variants on each protein position (the darker the colour, the higher the gMVP score). The bottom histogram shows the evolutionary conservation measured with the Kullback–Leibler divergence between amino acid distribution among homologous sequences and amino acid distribution in nature.

uses co-evolution strength to effectively pool information from potential three-dimensional neighbours. Used as edge features in a graph attention model, co-evolution strength allows more precise pooling of information from distant residues than the convolutional layer without prior structure. Co-evolution information has been used by previous methods for predicting functional impact of missense variants, such as PIVOTAL²⁵, a supervised ensemble predictor that combines scores from existing methods and EVmutation, an unsupervised method that learns co-evolution and conservation using Markov random fields from multi-sequence alignments (MSAs). Moreover, co-evolution information has been used in ab initio protein structure prediction extensively^{32,54,57}. The extraordinary performance of AlphaFold^{55,58}

in CASP14 shows that it contains critical information about physical residue–residue distances for accurate structure prediction of most proteins in the human proteome. The language model Transformer³³ has more recently been applied on protein sequences and MSAs to improve the performance of co-evolution strength estimation and protein residue–residue contacts prediction^{59–61}. gMVP could be further improved by integrating components of Transformer and protein three-dimensional structures in the model. On the other hand, MSA-based methods are limited for the proteins with no or few homologous sequences and could be improved by integrating the learned representations on large-scale unlabelled sequence data using sequence language modelling⁶⁰.

With transfer learning, the trained gMVP model can be further optimized for more specific tasks in genetic studies. The idea is to transfer the general knowledge learned from large training datasets to a new related and more specific task with only limited training data. The trained model can set the initial values of the weights in the model to be updated by further training to explore only a subspace of the whole parameter space. We have shown its feasibility in classifying GOF and LOF variants in the ion-channel genes using a limited number of training data points without additional prediction features. We expect that with transfer learning, gMVP can potentially improve variant interpretation by training gene family-specific models⁶² and identifying disease-specific damaging variants⁶³.

Functional readout data from deep mutational scan provides strong evidence of classifying variants as damaging or neutral^{27–30,64,65}. However, these in vitro functional readout assays usually reveal only one aspect of a protein's function in a limited number of cell types; therefore, they are often not completely correlated with the functional impact of the variants in vivo. We expect that more comprehensive deep mutational scan assays will become available and facilitate substantial improvement in the training and evaluation of computational methods.

Finally, we showed that although evolutionary conservation remains one of the most informative sources for computational methods, selection in humans can provide complementary information for prediction. The selection coefficient is correlated with allele frequency, especially for variants under strong negative selection^{46,66–68}. Larger population genome datasets can further improve estimation of allele frequency of rare variants. We anticipate large⁶⁹ and diverse⁷⁰ population genome data released in the future will improve estimation of selection effect in human and in turn improve gMVP.

Methods

Training datasets

For the positive training set, we collected: 22,607 variants from ClinVar database³⁷ under the pathogenic and likely pathogenic categories with a review status of at least one star; 48,125 variants from the Human Gene Mutation Database Pro v.2013 (HGMD) database³⁶ under the disease mutation category; and 20,481 variants from UniProt labelled as disease-causing. For the negative training set, we collected 41,185 variants from ClinVar under the benign and likely benign categories, and 33,387 variants from SwissVar³⁸ labelled as polymorphism. After excluding 3,751 variants with conflicting interpretations from the three databases, we have 63,304 and 66,102 unique positives and negatives, respectively. We next excluded 36,499 common variants (653 positives and 35,846 negatives) with an allele frequency $>1 \times 10^{-3}$ in gnomAD (all populations)⁴⁸ and 3,080 overlapping variants (2,680 positives and 400 negatives) with testing datasets from the training dataset, resulting in a dataset of 59,701 positives and 29,856 negatives. To balance the positive and negative training samples, we randomly selected 29,845 rare missense variants from the DiscovEHR database⁴³ that are not already covered by previously selected training data as additional negative training points. In the end we have 59,701 and 59,701 unique positive and negative training variants (Supplementary Table 1), which cover 3,463 and 14,222 genes, respectively.

Testing datasets

- (1) Cancer somatic mutation hotspots: we obtained 878 missense variants located in somatic missense mutations hotspots in 209 cancer driver genes from a recent study²⁶ as positives, and randomly selected twofold more rare missense variants ($N = 1,756$) from the population sequencing data DiscovEHR⁴³.
- (2) Functional readout data from deep mutational scan experiments: we compiled variants in *BRCA1*²⁸, *PTEN*²⁹, *TP53*³⁰ and *MSH2*²⁷. Findly and colleagues³⁰ applied genome editing to measure the functional consequences of all possible single nucleotide variants (SNVs) in key regions of *BRCA1*, where the functional

scores measured the SNV effects on the cell survival of the cloned cells. Mighell et al.²⁹ used a yeast model to systematically evaluate the effect of *PTEN* mutations on lipid phosphatase activity in vivo. Kotler et al.³⁰ created a synthetically designed library and measured the functional impact of the DNA-binding domain *p53* variants in human cells in culture and in vivo. Jia et al.²⁷ developed a human cell line model for *MSH2* to measure the chemical selection for mismatch repair dysfunction. The functional scores for *PTEN* and *BRCA1* correlate negatively, whereas the functional scores for *TP53* and *MSH2* correlate positively, with the pathogenicity of the variants, respectively. We used the suggested thresholds of the functional scores to label the positives and negatives for the variants. We only include the SNVs for comparison as most published methods do not provide scores for the non-SNVs. There are 432 positives and 1,476 negatives in *BRCA1*; 258 positives and 1,601 negatives in *PTEN*; 540 positives and 1,108 negatives in *TP53*; and 414 positives and 5,439 negatives in *MSH2*.

- (3) DNMs: to evaluate utility in new risk gene discovery, we used published rare germline DNMs from 5,924 cases and 2,007 controls in an ASD study⁴ and 31,058 cases in a neural developmental study⁵.

To fairly compare our methods with published methods, we excluded the overlapping variants with testing datasets from the training datasets. We further excluded all variants in *PTEN*, *TP53*, *BRCA1* and *MSH2* in training to avoid inflation in performance evaluation.

Past published methods included for comparison

We compared gMVP with PrimateAI, MPC, REVEL, M-CAP, MVP, ClinPred, BayesDel, EVmutation, SIFT, PolyPhen2, SIFT, phastCons⁷¹ and GERP. We calculated scores of EVmutation using its public software package (<https://github.com/debbiemarkslab/EVmutation>). We used the pre-computed scores of other methods compiled by dbNSFP. We annotated the variants in the testing test with these scores using VEP plug-in for dbNSFP.

The graph attention neural network model

gMVP uses a graph to represent a variant and its protein context. We first defined the 128 amino acids flanking the reference amino acid as protein context. We next built a star-like graph with the reference amino acid as the centre node and the flanking amino acids as context nodes, and with edges between the centre node and each context node (Fig. 1 and Supplementary Fig. 1).

Let \mathbf{x} , \mathbf{n} , and \mathbf{f}_i denote input feature vectors for the centre node, each context node and each edge, respectively. We first used three one-depth dense layers to encode \mathbf{x} , \mathbf{n} , and \mathbf{f}_i to latent representation vectors \mathbf{h} , \mathbf{t}_i and \mathbf{e}_i , respectively. We used RELU⁷² as the activation function and 512 neurons for each dense layer.

We then used a multi-head layer adapted from the attention layer in the Transformer model³³ to pool information from context nodes and finally to learn a context vector \mathbf{c} . Specifically, for the k th head, we first calculated the value vectors for each context node by $\mathbf{v}_i^{(k)} = \hat{\mathbf{W}}^{(k)} \mathbf{t}_i$. We next calculated attention scores for each context node through $s_i^k = \tanh(\mathbf{W}^{(k)} [\mathbf{h}, \mathbf{e}_i, \mathbf{t}_i]) + p_i$, where \tanh denotes a hyperbolic tangent activation function and p_i is a position bias, which is a simplified positional encoding⁷³. We note here that p_i allows the model to capture local protein sequence context. Attention weights are calculated by applying a softmax operation on the attention scores, $[\mathbf{w}_0^{(k)}, \dots, \mathbf{w}_i^{(k)}, \dots] = \text{softmax}([\mathbf{s}_0^{(k)}, \dots, \mathbf{s}_i^{(k)}, \dots])$.

The context vector $\mathbf{c}^{(k)}$ for the k th head is calculated as $\mathbf{c}^{(k)} = \sum \mathbf{w}_i^{(k)} \mathbf{v}_i^{(k)}$. The final context vector is obtained by a linear projection on the concatenation vector of the context vectors from each head,

$$\mathbf{c} = \mathbf{W}_p [\mathbf{c}^{(0)}, \dots, \mathbf{c}^{(l)}, \dots, \mathbf{c}^{(K-1)}].$$

Here K denotes the number of heads and we used four heads in our model. And we note that in the model, $\mathbf{W}_{(k)}$, $\hat{\mathbf{W}}^{(k)}$ and \mathbf{W}_p are weight matrices to be trained.

We next used a gated recurrent unit layer³⁵ to leverage the context vector \mathbf{c} and the latent vector \mathbf{h} of the given variant where the relative importance of the whole context can be determined. We used 512 neurons and a hyperbolic tangent activation function for the gated recurrent unit layer. We finally used a linear projection layer and a sigmoid layer to perform classification.

Input features

The centre node, which represents the variant, has the following features: reference and alternate amino acids, evolutionary conservation and predicted local structural properties. The context nodes have the following features: reference amino acids, evolutionary conservation, predicted local structural properties and observed and expected missense alleles in gnomAD⁴⁸. The feature of edges is co-evolution strength between the position of variant and other positions, estimated from multiple sequence alignments of homologous sequences.

Reference and alternate amino acids (40 values): we used one-hot encoding with a dimension of 20 to represent reference and alternate amino acids.

Protein primary sequence (20 values): we also used one-hot encoding to represent each amino acid in the protein primary sequence.

Evolutionary conservation (42 values): we estimated the evolutionary conservation from two sources: (1) we searched the homologous of the protein of interest against SwissProt database⁷⁴ with three iterations of search and then built the MSAs with HHblits suite⁷⁵; (2) we downloaded the MSAs of 200 species from Ensembl website for each human protein sequence⁷⁶. We then calculated the frequencies of 20 amino acids and the gap for each position for the two MSAs separately and concatenated the two frequency vectors.

Predicted protein structural properties (five values): we predicted the protein secondary structures (three values), solvent accessibility (one value) and the probability of a residue participating in interactions with other proteins (one value) using NetsurfP⁷⁷.

Observed number of missense alleles in gnomAD and expected number (two values): to capture selection effect in human, we obtained the observed number of rare missense variants in gnomAD⁴⁸ and the expected number of rare missense variants estimated using a background mutation model⁴⁸.

Co-evolution strength (442 values): we extract pairwise statistics from the MSA as co-evolution strength. It is estimated based on the covariance matrix constructed from the input MSA. First, we compute one- and two-site frequency counts $f_i(A) = \frac{1}{M} \sum_{m=1}^M \delta_{A, X_{i,m}}$ and $f_{ij}(A, B) = \frac{1}{M} \sum_{m=1}^M \delta_{A, X_{i,m}} \delta_{B, X_{j,m}}$ where A and B denote amino acid identities (20 + gap); δ is the Kronecker delta; i and j are position indexes on the aligned protein sequence; m is the sequence index of the MSA with a total of M aligned sequences; and $X_{i,m}$ indicates the amino acid identity of position i on sequence m . We then calculate the sample covariance (21×21) matrix $c_{ij}^{A,B} = f_{ij}(A, B) - f_i(A)f_j(B)$ and flatten it into a vector with 441 elements. We also convert the covariance matrix to a single value by computing its Frobenius norm $s_{ij} = \sqrt{\sum_{A=1}^{20} \sum_{B=1}^{20} (c_{ij}^{A,B})^2}$ and then concatenate the norm and the flattened vector as the edge features.

We built these features only for canonical transcripts defined by Ensembl⁷⁸ v.92. We annotated the variants using VEP⁷⁹.

Training algorithm

We used cross-entropy loss as the training loss. We used the Adam algorithm³⁹ to update the model parameters with an initial learning rate of 1×10^{-3} and decayed the learning rate with a polynomial decay schedule⁸⁰. We randomly selected 10% of training samples as validation set and early stopping was applied with validation loss as a watching metric. We trained five models by repeating the above training process

five times, and for testing, we averaged the outputs of the five models as prediction scores. The model and training algorithm were implemented using TensorFlow⁴⁰.

Classifying GOF and LOF variants using transfer learning. To investigate the potential for transfer learning, we further trained gMVP to classify GOF and LOF variants in ion-channel genes with additional training data but without new features. We collected 1,517 pathogenetic and 2,328 neutral variants in *SCNxA* genes, which encode voltage-gated sodium and calcium channel proteins, in which 518 and 309 variants are inferred as LOF and GOF variants, respectively, from a recent study⁴⁷.

We first trained a model, gMVP-TL1, to classify pathogenetic and neutral variants in *SCNxA* genes. We used the same dataset as funNCion⁴⁷, including 3,466 variants for training and 379 variants for testing. We randomly selected 10% variants from training set as validation set. We used the same model architecture with gMVP and initialized weights of the new model with the weights of original gMVP model. In the new model training, we used Adam to update the parameters at an initial learning rate of 1×10^{-3} and used the validation loss as stopping criteria. We trained five gMVP-TL1 models, starting from each of the five trained gMVP models, and for testing, we averaged the outputs of these models as prediction scores.

We next trained another model gMVP-TL2 to classify GOF versus LOF variants in *SCNxA* genes. We used 744 variants as training set and 81 variants as testing set, which are the same sets used by funNCion⁴⁷. Like gMVP-TL1, gMVP-TL2 were also trained starting from the weights of gMVP model previously trained using all genes. We used the same hyperparameter settings with gMVP-TL1 in training.

Normalization of scores using rank percentile

For each method, we first sorted predicted scores of all possible rare missense variants across all protein-coding genes and then converted the scores into rank percentiles. The higher rank percentile indicates more damaging, for example, a rank score of 0.9 indicates the missense variant is more likely to be damaging than 90% of all possible missense variants.

Precision–recall–proxy curves

As there are no ground-truth data to benchmark our performance on DNMs, we estimate precision and recall at various thresholds based on the enrichment of predicted damaging variants in cases compared to controls.

Let S_1 be the rate of synonymous variants in cases and S_0 be the rate of synonymous variants in controls. Then the synonymous rate ratio α is defined as

$$\alpha = \frac{S_1}{S_0}$$

Denote the total number of variants in cases as N_1 , the number of variants in controls as N_0 , the number of variants predicted as pathogenic in cases as M_1 and the number of variants predicted as pathogenic in controls as M_0 . We assume that for there to be no batch effect, the rate of synonymous variants should be the same in the cases and controls. So, we estimate the enrichment of predicted pathogenic variants in cases compared to controls by:

$$R = \frac{\frac{M_1}{N_1}}{\frac{M_0}{N_0}} \times \alpha$$

The true number of pathogenic DNMs M_1' is then estimated by

$$M_1' = \frac{M_1(R-1)}{R}$$

And the estimated precision is

$$\widehat{\text{Precision}} = \frac{M'_1}{M_1}$$

Reporting summary

Further information on research design is available in the Nature Portfolio Reporting Summary linked to this article.

Data availability

Pre-computed gMVP scores for all possible missense variants in canonical transcripts on human hg38 can be downloaded from <https://www.dropbox.com/s/nce1jhg3i7jw1hx/gMVP.2021-02-28.csv.gz?dl=0>. The training data of the main model were downloaded from <http://www.discovehrshare.com/downloads> (DiscovEHR), <http://www.hgmd.cf.ac.uk/ac/index.php> (HGMD), <https://www.uniprot.org/docs/humpvar> (UniProt) and https://ftp.ncbi.nlm.nih.gov/pub/clinvar/vcf_GRCh37/ (ClinVar). Other datasets supporting the findings of this study are available in the paper and the Supplementary Information.

Code availability

The codes for the model design and training and testing procedure are available on GitHub (<https://github.com/ShenLab/gMVP/>) and Zenodo⁸¹.

References

- Boettcher, S. et al. A dominant-negative effect drives selection of TP53 missense mutations in myeloid malignancies. *Science* **365**, 599–604 (2019).
- Huang, K. L. et al. Pathogenic germline variants in 10,389 adult cancers. *Cell* **173**, 355–370.e14 (2018).
- Jin, S. C. et al. Contribution of rare inherited and de novo variants in 2,871 congenital heart disease probands. *Nat. Genet.* **49**, 1593–1601 (2017).
- Satterstrom, F. K. et al. Large-scale exome sequencing study implicates both developmental and functional changes in the neurobiology of autism. *Cell* **180**, 568–584.e23 (2020).
- Kaplanis, J. et al. Evidence for 28 genetic disorders discovered by combining healthcare and research data. *Nature* **586**, 757–762 (2020).
- Rehm, H. L., Berg, J. S. & Plon, S. E. ClinGen and ClinVar—enabling genomics in precision medicine. *Hum. Mutat.* **39**, 1473–1475 (2018).
- He, X. et al. Integrated model of de novo and inherited genetic variants yields greater power to identify risk genes. *PLoS Genet.* **9**, e1003671 (2013).
- Nguyen, H. T. et al. Integrated Bayesian analysis of rare exonic variants to identify risk genes for schizophrenia and neurodevelopmental disorders. *Genome Med.* **9**, 114 (2017).
- Adzhubei, I., Jordan, D. M. & Sunyaev, S.R. Predicting functional effect of human missense mutations using PolyPhen-2. *Curr. Protoc. Hum. Genet.* <https://doi.org/10.1002/0471142905.hg0720s76> (2013).
- Carter, H., Douville, C., Stenson, P. D., Cooper, D. N. & Karchin, R. Identifying Mendelian disease genes with the variant effect scoring tool. *BMC Genom.* **14**, S3 (2013).
- Kircher, M. et al. A general framework for estimating the relative pathogenicity of human genetic variants. *Nat. Genet.* **46**, 310–315 (2014).
- Ioannidis, N. M. et al. REVEL: an ensemble method for predicting the pathogenicity of rare missense variants. *Am. J. Hum. Genet.* **99**, 877–885 (2016).
- Dong, C. et al. Comparison and integration of deleteriousness prediction methods for nonsynonymous SNVs in whole exome sequencing studies. *Hum. Mol. Genet.* **24**, 2125–2137 (2015).
- Jagadeesh, K. A. et al. M-CAP eliminates a majority of variants of uncertain significance in clinical exomes at high sensitivity. *Nat. Genet.* **48**, 1581–1586 (2016).
- Ionita-Laza, I., McCallum, K., Xu, B. & Buxbaum, J. D. A spectral approach integrating functional genomic annotations for coding and noncoding variants. *Nat. Genet.* **48**, 214–220 (2016).
- Qi, H. et al. MVP predicts the pathogenicity of missense variants by deep learning. *Nat. Commun.* **12**, 510 (2021).
- Sundaram, L. et al. Predicting the clinical impact of human mutation with deep neural networks. *Nat. Genet.* **50**, 1161 (2018).
- Samocha, K.E. et al. Regional missense constraint improves variant deleteriousness prediction. Preprint at *bioRxiv* <https://doi.org/10.1101/148353> (2017).
- Havrilla, J. M., Pedersen, B. S., Layer, R. M. & Quinlan, A. R. A map of constrained coding regions in the human genome. *Nat. Genet.* **51**, 88–95 (2019).
- Davydov, E. V. et al. Identifying a high fraction of the human genome to be under selective constraint using GERP plus. *PLoS Comput. Biol.* **6**, e1001025 (2010).
- Iqbal, S. et al. Comprehensive characterization of amino acid positions in protein structures reveals molecular effect of missense variants. *Proc. Natl Acad. Sci. USA* **117**, 28201–28211 (2020).
- Hicks, M., Bartha, I., di Iulio, J., Venter, J. C. & Telenti, A. Functional characterization of 3D protein structures informed by human genetic diversity. *Proc. Natl Acad. Sci. USA* **116**, 8960–8965 (2019).
- Sivley, R. M., Dou, X. Y., Meiler, J., Bush, W. S. & Capra, J. A. Comprehensive analysis of constraint on the spatial distribution of missense variants in human protein structures. *Am. J. Hum. Genet.* **102**, 415–426 (2018).
- Hopf, T. A. et al. Mutation effects predicted from sequence co-variation. *Nat. Biotechnol.* **35**, 128–135 (2017).
- Liang, S., Mort, M., Stenson, P.D., Cooper, D.N. & Yu, H. PIVOTAL: prioritizing variants of uncertain significance with spatial genomic patterns in the 3D proteome. Preprint at *bioRxiv* <https://doi.org/10.1101/2020.06.04.135103> (2021).
- Chang, M. T. et al. Accelerating discovery of functional mutant alleles in cancer. *Cancer Discov.* **8**, 174–183 (2018).
- Jia, X. et al. Massively parallel functional testing of MSH2 missense variants conferring Lynch syndrome risk. *Am. J. Hum. Genet.* **108**, 163–175 (2021).
- Findlay, G. M. et al. Accurate classification of BRCA1 variants with saturation genome editing. *Nature* **562**, 217–222 (2018).
- Mighell, T. L., Evans-Dutson, S. & O’Roak, B. J. A saturation mutagenesis approach to understanding PTEN lipid phosphatase activity and genotype–phenotype relationships. *Am. J. Hum. Genet.* **102**, 943–955 (2018).
- Kotler, E. et al. A systematic p53 mutation library links differential functional impact to cancer mutation pattern and evolutionary conservation. *Mol. Cell* **71**, 178–190.e8 (2018).
- de Juan, D., Pazos, F. & Valencia, A. Emerging methods in protein co-evolution. *Nat. Rev. Genet.* **14**, 249–261 (2013).
- Morcos, F. et al. Direct-coupling analysis of residue coevolution captures native contacts across many protein families. *Proc. Natl Acad. Sci. USA* **108**, E1293–E1301 (2011).
- Vaswani, A. et al. Attention is all you need. In *31st Conference on Neural Information Processing Systems* 5998–6008 (NeurIPS, 2017).
- Veličković, P. et al. Graph attention networks. In *6th International Conference on Learning Representations* (Univ. Cambridge, 2018).
- Cho, K. et al. Learning phrase representations using RNN encoder–decoder for statistical machine translation. In *Proc. 2014 Conference on Empirical Methods in Natural Language Processing* (Association for Computational Linguistics, 2014).

36. Stenson, P. D. et al. Human gene mutation database (HGMD (R)): 2003 update. *Hum. Mutat.* **21**, 577–581 (2003).
37. Landrum, M. J. et al. ClinVar: public archive of relationships among sequence variation and human phenotype. *Nucl. Acids Res.* **42**, D980–D985 (2014).
38. Mottaz, A., David, F. P., Veuthey, A. L. & Yip, Y. L. Easy retrieval of single amino-acid polymorphisms and phenotype information using SwissVar. *Bioinformatics* **26**, 851–852 (2010).
39. Kingma, D. P. & Ba, J. Adam: a method for stochastic optimization. In *2015 International Conference on Learning Representations (ICLR, 2015)*.
40. Abadi, M. et al. TensorFlow: large-scale machine learning on heterogeneous distributed systems. Preprint at <https://arxiv.org/abs/1603.04467> (2016).
41. Alirezaie, N., Kernohan, K. D., Hartley, T., Majewski, J. & Hocking, T. D. ClinPred: prediction tool to identify disease-relevant nonsynonymous single-nucleotide variants. *Am. J. Hum. Genet.* **103**, 474–483 (2018).
42. Feng, B. J. PERCH: a unified framework for disease gene prioritization. *Hum. Mutat.* **38**, 243–251 (2017).
43. Dewey, F. E. et al. Distribution and clinical impact of functional variants in 50,726 whole-exome sequences from the DiscovEHR Study. *Science* **354**, eaf6814 (2016).
44. Iossifov, I. et al. The contribution of de novo coding mutations to autism spectrum disorder. *Nature* **515**, 216–221 (2014).
45. De Rubeis, S. et al. Synaptic, transcriptional and chromatin genes disrupted in autism. *Nature* **515**, 209–215 (2014).
46. Zuk, O. et al. Searching for missing heritability: designing rare variant association studies. *Proc. Natl Acad. Sci. USA* **111**, E455–E464 (2014).
47. Heyne, H. O. et al. Predicting functional effects of missense variants in voltage-gated sodium and calcium channels. *Sci. Transl. Med.* **12**, eaay6848 (2020).
48. Karczewski, K. J. et al. The mutational constraint spectrum quantified from variation in 141,456 humans. *Nature* **581**, 434–443 (2020).
49. Abrusán, G. & Marsh, J. A. Alpha helices are more robust to mutations than beta strands. *PLoS Comput. Biol.* **12**, e1005242 (2016).
50. Gao, M., Zhou, H. & Skolnick, J. Insights into disease-associated mutations in the human proteome through protein structural analysis. *Structure* **23**, 1362–1369 (2015).
51. Li, S.-C., Goto, N. K., Williams, K. A. & Deber, C. M. Alpha-helical, but not beta-sheet, propensity of proline is determined by peptide environment. *Proc. Natl Acad. Sci. USA* **93**, 6676–6681 (1996).
52. Senior, A. W. et al. Improved protein structure prediction using potentials from deep learning. *Nature* **577**, 706–710 (2020).
53. Yang, J. Y. et al. Improved protein structure prediction using predicted interresidue orientations. *Proc. Natl Acad. Sci. USA* **117**, 1496–1503 (2020).
54. Wang, S., Sun, S., Li, Z., Zhang, R. & Xu, J. Accurate de novo prediction of protein contact map by ultra-deep learning model. *PLoS Comput. Biol.* **13**, e1005324 (2017).
55. Jumper, J. et al. Highly accurate protein structure prediction with AlphaFold. *Nature* **596**, 583–589 (2021).
56. Kumar, S., Clarke, D. & Gerstein, M. B. Leveraging protein dynamics to identify cancer mutational hotspots using 3D structures. *Proc. Natl Acad. Sci. USA* **116**, 18962–18970 (2019).
57. Anishchenko, I., Ovchinnikov, S., Kamisetty, H. & Baker, D. Origins of coevolution between residues distant in protein 3D structures. *Proc. Natl Acad. Sci. USA* **114**, 9122–9127 (2017).
58. Tunyasuvunakool, K. et al. Highly accurate protein structure prediction for the human proteome. *Nature* **596**, 590–596 (2021).
59. Rao, R. et al. MSA transformer. In *Proc. 38th International Conference on Machine Learning* 8844–8856 (PMLR, 2021).
60. Rives, A. et al. Biological structure and function emerge from scaling unsupervised learning to 250 million protein sequences. *Proc. Natl Acad. Sci. USA* **118**, e2016239118 (2021).
61. Rao, R., Meier, J., Sercu, T., Ovchinnikov, S. & Rives, A. Transformer protein language models are unsupervised structure learners. In *2015 International Conference on Learning Representations (ICLR, 2015)*.
62. Lal, D. et al. Gene family information facilitates variant interpretation and identification of disease-associated genes in neurodevelopmental disorders. *Genome Med.* **12**, 28 (2020).
63. Zhang, X. et al. Disease-specific variant pathogenicity prediction significantly improves variant interpretation in inherited cardiac conditions. *Genet. Med.* **23**, 69–79 (2021).
64. Starita, L. M. et al. Variant interpretation: functional assays to the rescue. *Am. J. Human Genet.* **101**, 315–325 (2017).
65. Brnich, S. E. et al. Recommendations for application of the functional evidence PS3/BS3 criterion using the ACMG/AMP sequence variant interpretation framework. *Genome Med.* **12**, 3 (2019).
66. Hartl, D. L. & Clark, A. G. *Principles of Population Genetics* 4th edn (Sinauer Associates, 1989).
67. Cassa, C. A. et al. Estimating the selective effects of heterozygous protein-truncating variants from human exome data. *Nat. Genet.* **49**, 806–810 (2017).
68. Charlesworth, B. & Hill, W. G. Selective effects of heterozygous protein-truncating variants. *Nat. Genet.* **51**, 2 (2019).
69. Bycroft, C. et al. The UK Biobank resource with deep phenotyping and genomic data. *Nature* **562**, 203–209 (2018).
70. Mulder, N. et al. H3Africa: current perspectives. *Pharmgenomics Pers. Med.* **11**, 59–66 (2018).
71. Siepel, A. et al. Evolutionarily conserved elements in vertebrate, insect, worm, and yeast genomes. *Genome Res.* **15**, 1034–1050 (2005).
72. Glorot, X., Bordes, A. & Bengio, Y. Deep sparse rectifier neural networks. In *Proc. 14th International Conference on Artificial Intelligence and Statistics* 315–323 (JMLR, 2011).
73. Ke, G., He, D. & Liu, T.-Y. Rethinking positional encoding in language pre-training. In *2021 International Conference on Learning Representations (ICLR, 2021)*.
74. Bateman, A. Uniprot: a universal hub of protein knowledge. *Protein Sci.* **28**, 32–32 (2019).
75. Remmert, M., Biegert, A., Hauser, A. & Soding, J. HHblits: lightning-fast iterative protein sequence searching by HMM-HMM alignment. *Nat. Methods* **9**, 173–175 (2012).
76. Herrero, J. et al. Ensembl comparative genomics resources. *Database* **2016**, bav096 (2016).
77. Klausen, M. S. et al. NetSurfP-2.0: improved prediction of protein structural features by integrated deep learning. *Proteins* **87**, 520–527 (2019).
78. Armean, I. M. et al. Enhanced access to extensive phenotype and disease annotation of genes and genetic variation in Ensembl. *Eur. J. Human Genet.* **27**, 1721–1721 (2019).
79. McLaren, W. et al. The Ensembl variant effect predictor. *Genome Biol.* **17**, 122 (2016).
80. Ge, R., Kakade, S. M., Kidambi, R. & Netrapalli, P. Rethinking learning rate schedules for stochastic optimization. In *2019 International Conference on Learning Representations (ICLR, 2019)*.
81. Zhang, H. & Shen, Y. ShenLab/gMVP: v1.0.0-alpha. *Zenodo* <https://doi.org/10.5281/zenodo.7134878> (2022).

Acknowledgements

This work was supported by NIH grants (nos. R01GM120609, R03HL147197, U01HG008680 and K99HG011490) and the Columbia

University Precision Medicine Joint Pilot Grants Program. We thank Y. Zhao, G. Zhong, M. AlQuraishi and D. Knowles for helpful discussions.

Author contributions

Y.S. conceived and guided the study. H.Z. implemented the algorithms and performed the main analyses. All authors contributed to data analysis, interpretation and manuscript writing.

Competing interests

The authors declare no competing interests.

Additional information

Supplementary information The online version contains supplementary material available at <https://doi.org/10.1038/s42256-022-00561-w>.

Correspondence and requests for materials should be addressed to Yufeng Shen.

Peer review information *Nature Machine Intelligence* thanks Xiaoming Liu, Wim Vranken, Amit R Majithia and the other, anonymous, reviewer(s) for their contribution to the peer review of this work.

Reprints and permissions information is available at www.nature.com/reprints.

Publisher's note Springer Nature remains neutral with regard to jurisdictional claims in published maps and institutional affiliations.

Springer Nature or its licensor (e.g. a society or other partner) holds exclusive rights to this article under a publishing agreement with the author(s) or other rightsholder(s); author self-archiving of the accepted manuscript version of this article is solely governed by the terms of such publishing agreement and applicable law.

© The Author(s), under exclusive licence to Springer Nature Limited 2022

Reporting Summary

Nature Portfolio wishes to improve the reproducibility of the work that we publish. This form provides structure for consistency and transparency in reporting. For further information on Nature Portfolio policies, see our [Editorial Policies](#) and the [Editorial Policy Checklist](#).

Statistics

For all statistical analyses, confirm that the following items are present in the figure legend, table legend, main text, or Methods section.

n/a	Confirmed
<input type="checkbox"/>	<input checked="" type="checkbox"/> The exact sample size (n) for each experimental group/condition, given as a discrete number and unit of measurement
<input checked="" type="checkbox"/>	<input type="checkbox"/> A statement on whether measurements were taken from distinct samples or whether the same sample was measured repeatedly
<input type="checkbox"/>	<input checked="" type="checkbox"/> The statistical test(s) used AND whether they are one- or two-sided <i>Only common tests should be described solely by name; describe more complex techniques in the Methods section.</i>
<input checked="" type="checkbox"/>	<input type="checkbox"/> A description of all covariates tested
<input type="checkbox"/>	<input checked="" type="checkbox"/> A description of any assumptions or corrections, such as tests of normality and adjustment for multiple comparisons
<input type="checkbox"/>	<input checked="" type="checkbox"/> A full description of the statistical parameters including central tendency (e.g. means) or other basic estimates (e.g. regression coefficient) AND variation (e.g. standard deviation) or associated estimates of uncertainty (e.g. confidence intervals)
<input type="checkbox"/>	<input checked="" type="checkbox"/> For null hypothesis testing, the test statistic (e.g. F , t , r) with confidence intervals, effect sizes, degrees of freedom and P value noted <i>Give P values as exact values whenever suitable.</i>
<input checked="" type="checkbox"/>	<input type="checkbox"/> For Bayesian analysis, information on the choice of priors and Markov chain Monte Carlo settings
<input checked="" type="checkbox"/>	<input type="checkbox"/> For hierarchical and complex designs, identification of the appropriate level for tests and full reporting of outcomes
<input type="checkbox"/>	<input checked="" type="checkbox"/> Estimates of effect sizes (e.g. Cohen's d , Pearson's r), indicating how they were calculated

Our web collection on [statistics for biologists](#) contains articles on many of the points above.

Software and code

Policy information about [availability of computer code](#)

Data collection	we used data from recent publications and public or commercial databases, all properly cited in the manuscript. We include a section "Data availability" in the manuscript describing the sources of the data sets used in the study. We did not generate new original data.
Data analysis	We used dbNSFP (version 4.0a) and VEP (version 92) to annotate the variants with scores of MVP, PrimateAI, REVEL, CADD, SIFT, phastCons, and MPC. It is all described in the manuscript.

For manuscripts utilizing custom algorithms or software that are central to the research but not yet described in published literature, software must be made available to editors and reviewers. We strongly encourage code deposition in a community repository (e.g. GitHub). See the Nature Portfolio [guidelines for submitting code & software](#) for further information.

Data

Policy information about [availability of data](#)

All manuscripts must include a [data availability statement](#). This statement should provide the following information, where applicable:

- Accession codes, unique identifiers, or web links for publicly available datasets
- A description of any restrictions on data availability
- For clinical datasets or third party data, please ensure that the statement adheres to our [policy](#)

1. Precomputed gMVP scores for all possible missense variants in canonical transcripts on human hg38 can be downloaded from:

<https://www.dropbox.com/s/nce1jhg3i7jw1hx/gMVP.2021-02-28.csv.gz?dl=0>.

2. The training data of the main model were downloaded from: <http://www.discovershare.com/downloads> (DiscovEHR), <http://www.hgmd.cf.ac.uk/ac/index.php> (HGMD), <https://www.uniprot.org/docs/humpvar> (UniProt), and https://ftp.ncbi.nlm.nih.gov/pub/clinvar/vcf_GRCh37/ (ClinVar).

3. Other data sets supporting the findings of this study are available in the manuscript and supplementary information files.

Human research participants

Policy information about [studies involving human research participants and Sex and Gender in Research](#).

Reporting on sex and gender	<input type="text" value="N/A."/>
Population characteristics	<input type="text" value="N/A."/>
Recruitment	<input type="text" value="N/A."/>
Ethics oversight	<input type="text" value="N/A."/>

Note that full information on the approval of the study protocol must also be provided in the manuscript.

Field-specific reporting

Please select the one below that is the best fit for your research. If you are not sure, read the appropriate sections before making your selection.

Life sciences Behavioural & social sciences Ecological, evolutionary & environmental sciences

For a reference copy of the document with all sections, see [nature.com/documents/nr-reporting-summary-flat.pdf](https://www.nature.com/documents/nr-reporting-summary-flat.pdf)

Life sciences study design

All studies must disclose on these points even when the disclosure is negative.

Sample size	<input type="text" value="N/A. This study does NOT deal with human subjects for estimating the effect size of a treatment. The statistical analyses have been reviewed based on the evidence from data that are available for each comparison."/>
Data exclusions	<input type="text" value="N/A. We did not exclude data as described in the study."/>
Replication	<input type="text" value="N/A. This is not an association study. The performance of the new method was evaluated by independent testing data sets from different sources."/>
Randomization	<input type="text" value="N/A. This is not a trial study."/>
Blinding	<input type="text" value="N/A."/>

Reporting for specific materials, systems and methods

We require information from authors about some types of materials, experimental systems and methods used in many studies. Here, indicate whether each material, system or method listed is relevant to your study. If you are not sure if a list item applies to your research, read the appropriate section before selecting a response.

Materials & experimental systems

n/a	<input type="checkbox"/> Involved in the study
<input checked="" type="checkbox"/>	<input type="checkbox"/> Antibodies
<input checked="" type="checkbox"/>	<input type="checkbox"/> Eukaryotic cell lines
<input checked="" type="checkbox"/>	<input type="checkbox"/> Palaeontology and archaeology
<input checked="" type="checkbox"/>	<input type="checkbox"/> Animals and other organisms
<input checked="" type="checkbox"/>	<input type="checkbox"/> Clinical data
<input checked="" type="checkbox"/>	<input type="checkbox"/> Dual use research of concern

Methods

n/a	<input type="checkbox"/> Involved in the study
<input checked="" type="checkbox"/>	<input type="checkbox"/> ChIP-seq
<input checked="" type="checkbox"/>	<input type="checkbox"/> Flow cytometry
<input checked="" type="checkbox"/>	<input type="checkbox"/> MRI-based neuroimaging